Single-layer broadband planar antenna using ultrathin high-efficiency focusing metasurfaces*

Hai-Sheng Hou(侯海生), Guang-Ming Wang(王光明)†, Hai-Peng Li(李海鹏), Wen-Long Guo(郭文龙), Tang-jing Li(李唐景), and Tong Cai(蔡通)‡

Air and Missile Defense College, Air Force Engineering University, Xi'an 710051, *China*

(Received 9 October 2016; revised manuscript received 7 December 2016; published online 30 March 2017)

Phase gradient metasurfaces (PGMS) offer a fascinating ability to control the amplitude and phase of the electromagnetic (EM) waves on a subwavelength scale, resulting in new applications of designing novel microwave devices with improved performances. In this paper, a reflective symmetrical element, consisting of orthogonally I-shaped structures, has been demonstrated with an approximately parallel phase response from 15 GHz to 22 GHz, which results in an interesting wideband property. For practical design, a planar antenna is implemented by a well-optimized focusing metasurface and excited by a self-designed Vivaldi antenna at the focus. Numerical and experimental results coincide well. The planar antenna has a series of merits such as a wide 3-dB gain bandwidth of 15–22 GHz, an average gain enhancement of 16 dB, a comparable aperture efficiency of better than 45% at 18 GHz, and also a simple fabrication process. The proposed reflective metasurface opens up a new avenue to design wideband microwave devices.

Keywords: phase gradient metasurfaces, ultrathin, broadband, focusing

PACS: 77.22.–d, 73.61.–r, 84.90.+a, 77.22.–d **DOI:** 10.1088/1674-1056/26/5/057701

1. Introduction

Recently, metasurfaces (MS) have attracted growing interests of many researchers due to their planar profile, easy fabrication, and also strong beam control capacity.[1–6] Phase gradient metasurfaces (PGMS), proposed by Yu *et al.*,[7] have found a wide range of applications, such as anomalous beam bending,[8–10] focusing,[11–13] and other optical devices. However, most reported metasurfaces suffer from a narrow bandwidth, which restricts their further applications, especially in planar antenna design. This is partly due to the inherent narrow band property of most phase shifting elements. To overcome this drawback, several methods have been proposed, such as using stacked phase shifting elements[14] or a patches aperture coupled to true-time delay lines.[15] To reduce the manufacturing cost of the multilayer planar antenna, a single-layer broadband planar antenna has been proposed.

The subwavelength element has been proposed. Due to the element with a subwavelength scale, a higher gain can be achieved compared to the elements with half a wavelength.[16] However, it is a challenge for the researchers to design a single-layer subwavelength element which spans a phase range larger than 360° for broadband.

In this paper, a single-layer symmetrical element with a cell size of 0.35λ at 18 GHz, consisting of orthogonally I-shaped metallic patterns, is proposed. By varying the length of the I-shape metallic, a phase variation range larger than 360° can be obtained from 15 GHz to 22 GHz, resulting in a parallel phase response within quite a broad bandwidth. A focusing metasurface based on the designed reflective element is optimized based on the commercial CST Microwave Studio. Excited by a Vivaldi antenna at the focal point, a wideband planar antenna is designed, fabricated, and measured. Numerical and experimental results coincide well. The planar antenna has a series of merits such as a wide 3-dB gain bandwidth of 15–22 GHz, an average gain enhancement of 16 dB, a comparable aperture efficiency of better than 45% at 18 GHz, and also a simple fabrication process. Finally, the whole paper is summarized.

2. Reflective phase gradient metasurface design

2.1. Element design with broad phase bandwidth

An element with a symmetrical structure is proposed as shown in Fig. 1. The element is composed of orthogonally I-shaped structures and a metal-grounded plane spaced by a dielectric isolator with the permittivity $\varepsilon_r = 2.65$, loss tangent 0.001, and thickness of 2 mm. The incoming waves will be totally reflected by the ground plane, namely, the reflection magnitude is close to 1 (0 dB), but the phases of the reflected waves can be modulated by the MS.[17] Full-wave simulation of the reflection phase versus length a is performed with commercial software CST Microwave Studio. The unit cell boundary conditions are employed along x and y directions. Moreover, the element is normally illuminated by a plane wave.

*Project supported by the National Natural Science Foundation of China (Grant No. 61372034).

†Corresponding author. E-mail: wgming01@sina.com

‡Corresponding author. E-mail: caitong326@sina.cn

© 2017 Chinese Physical Society and IOP Publishing Ltd

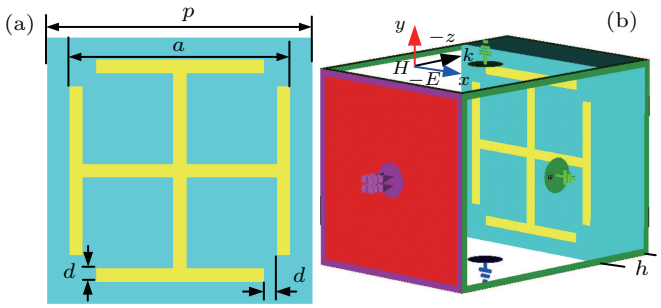


Fig. 1. (color online) Structure of the element and the simulated setup: (a) top view, (b) perspective view. The parameters are $d = 0.3$ mm, $p = 6$ mm, $h = 2$ mm, and $a = 1.8$–5 mm.

Figure 2 plots eight representative phase shift lines operating from 15 GHz to 22 GHz with the parameter a varying from 1.8 mm to 5.0 mm, which spans a phase range of larger than 360°. In addition, it is observed that an approximately constant phase slope is obtained for different operating frequencies, which enables the reflective element to have a large bandwidth.

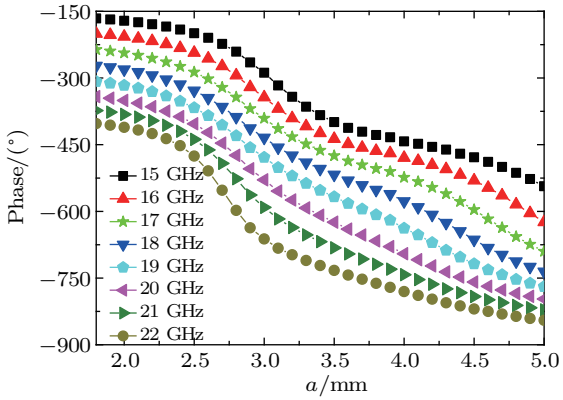


Fig. 2. (color online) Reflected phase shift versus a from 15 GHz to 22 GHz.

2.2. Broadband and ultrathin focusing PGMS design

As we know, the reflected wave will always deflect to the phase delay direction according to the general reflection law[7]

$$n_{\mathrm{r}}\sin(\theta_{\mathrm{r}}) - n_{\mathrm{i}}\sin(\theta_{\mathrm{i}}) = \frac{\lambda}{2\pi}\frac{\mathrm{d}\Phi}{\mathrm{d}x}, \tag{1}$$

where Φ is the phase discontinuity at a local position on the metasurface, θ_{r} (θ_{i}) is the reflected (incident) angle of the electromagnetic wave, n_{r} (n_{i}) is the reflective index of the reflected (incident) medium, and λ is the wavelength. Here, $\mathrm{d}\Phi/\mathrm{d}x$ can be described as $2\pi/(np)$, where n is the number of elements arranged in order along the x direction and p is the periodicity of the element. In the design, the EM wave normally impinges on the elements, thus θ_{i} is 0°. Considering that the element is placed in free space (i.e., $n_{\mathrm{i}} = 1$), we obtain the reflected angle θ_{r} as follows:

$$\theta_{\mathrm{r}} = \sin^{-1}\left(\frac{\lambda}{2\pi}\frac{2\pi}{np}\right). \tag{2}$$

Then we concentrate on designing a parabolic phase distribution on the focusing metasurface, which can focus the incident plane wave. According to Fermat's principle, the EM wavefront can be modified by controlling the phase distribution. For a given focal length L, in order to efficiently focus the incident plane wave to a quasi-spherical wave, the phase $\phi(m,n)$ imposed at element location (m,n) should satisfy the following equation:

$$\Phi(m,n) = \frac{2\pi}{\lambda}\left(\sqrt{(mp)^2 + (np)^2 + L^2} - L\right) + \Phi_0. \tag{3}$$

The schematic of the focusing effect is shown in Fig. 3(a). In fact, with a point source positioned at the focus, the conversion of a spherical wave to a plane wave can be achieved, which can be seen in Fig. 3(b).

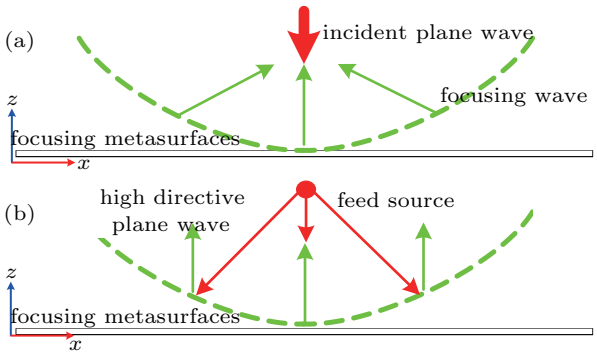


Fig. 3. (color online) (a) Schematic used to describe the focusing effect. (b) Schematic used to describe the operating mechanism of planar antenna.

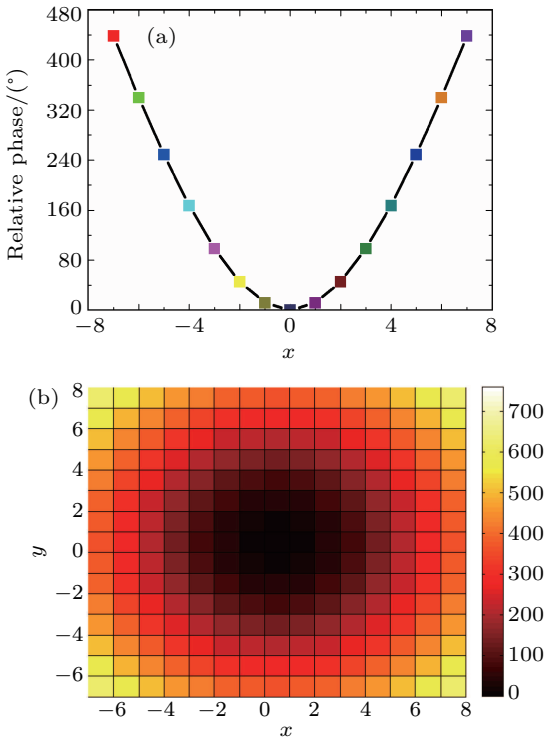


Fig. 4. (color online) (a) Phase response on the cut line along the x direction. (b) Relative reflection phase distribution in the xoy plane.

As shown in Fig. 4, a hyperbolic phase distribution is assigned on the MS, which will contribute to focusing the incident plane wave. By inserting Φ_0 and L into Eq. (3), we can obtain $\Phi(m,n)$ at the location (m, n). After that, the parameter a can be obtained according to Fig. 2. The focal length is set as $F = 33$ mm and the focal distance to diameter ratio (F/D) is calculated as 0.37. To efficiently collimate the spatial phase and achieve a high aperture efficiency, eight elements are used to cover 2π phase shift in the $+x$ direction as shown in Fig. 4(a). Moreover, as shown in Fig. 5(a), a focusing metasurface with a total size of 90 mm×90 mm is designed according to Eq. (3) and Fig. 4.

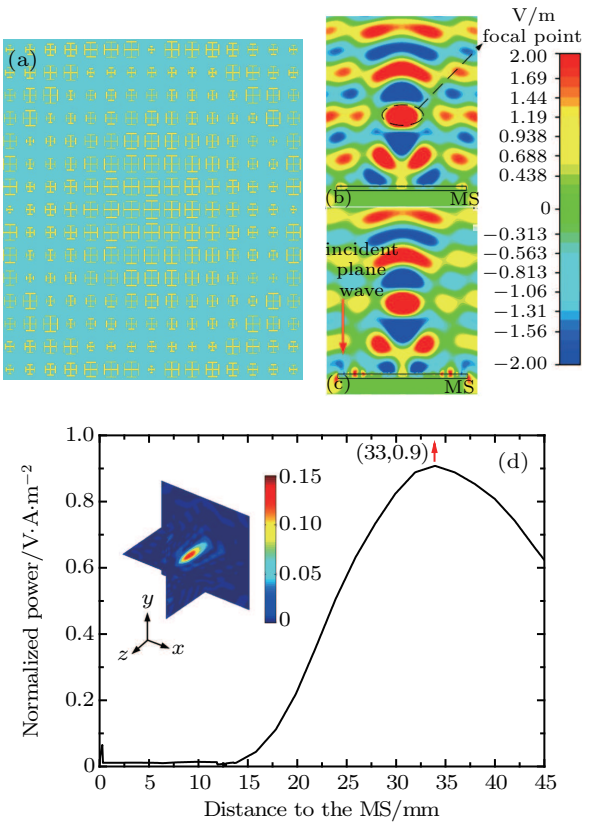


Fig. 5. (color online) (a) Simulated focusing MS. (b) Simulated reflected electric field distribution in *yoz*-plane at 18 GHz. (c) Simulated reflected electric field distribution in *xoz*-plane at 18 GHz. (d) Power distribution of focusing wave at 18 GHz and distance to the MS.

To provide an intuitionistic view on the focusing effect, the metasurface is illuminated by a plane wave with linear polarization propagating along the $-z$ direction in the *xoy*-plane. Figures 5(b) and 5(c) plot the electrical field at the center frequency 18 GHz at *xoz* and *yoz* planes, respectively. It can be seen clearly that the incident plane wave does converge to a point in the orthogonal planes. The excellent focusing effect results from the strong phase compensation capacity of the reflective metasurface. To verify the position of the focus, the energy distribution is simulated at the center frequency $f_0 = 18$ GHz, which is shown in Fig. 5(d). It can be seen clearly that the energy is focused at both *xoz* and *yoz* planes, just as the red spot shows. Moreover, a curve is put along the *z* direction and the power field is evaluated on the curve. The normalized power versus the distance to the MS is plotted in Fig. 5(d), indicating that the maximum energy nearly appears at 33 mm. Therefore, a conclusion can be drawn that the focal length is $F = 33$ mm, which agrees well with the theoretical calculation.

3. Broadband and high-gain planar antenna design

The proposed metasurface can be used to design a planar antenna with high gain and broad bandwidth. As we know, a spherical wave, emitted by a source located at the focal point of a focusing metasurface, can be transformed to a plane wave. Here, the feed antenna has been well designed with a wide operating bandwidth. The picture of the designed Vivaldi antenna is shown in Fig. 6. The reflection coefficient of the antenna is shown in Fig. 6(b). The designed antenna can operate from 15 GHz to 22 GHz with S_{11} lower than -10 dB, which can be adopted as a feed antenna. More importantly, the designed feed antenna has a small blockage for the planar antenna system compared to a horn antenna.

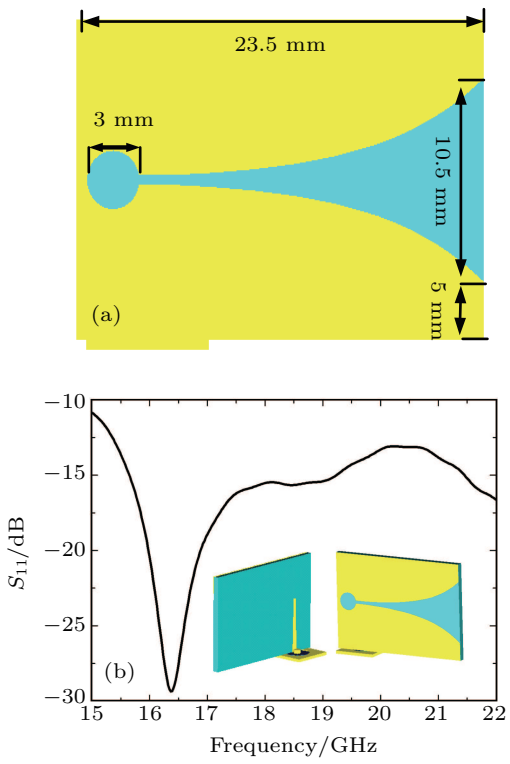


Fig. 6. (color online) (a) Parameters of Vivaldi antenna. (b) Simulated S_{11} of Vivaldi antenna.

To demonstrate the conversion from a spherical wave to a plane wave, the CST simulated electric field distributions at both *xoz* and *yoz* planes at three representative frequencies (15 GHz, 18 GHz, and 22 GHz) are plotted in Figs. 7–9. It is exciting to point out that the nearly flat plane wave above the MS in *xoz* and *yoz* is clearly seen as expected.

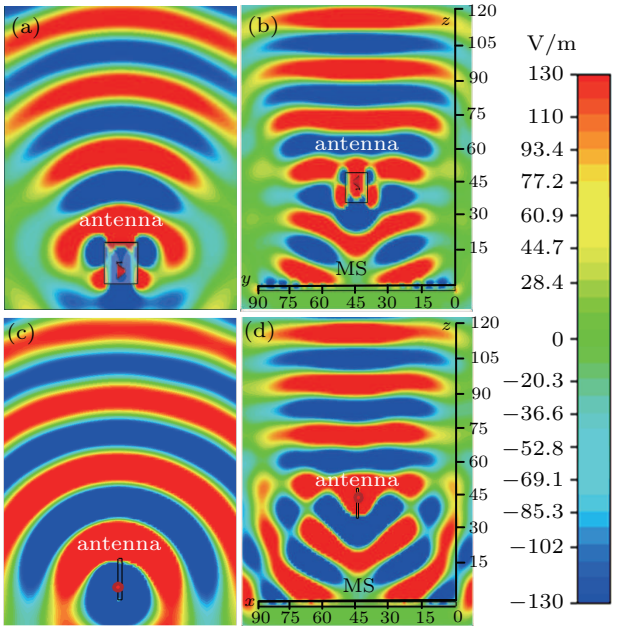


Fig. 7. (color online) Simulated electric field distribution at 15 GHz in (a), (b) *yoz*-plane and (c), (d) *xoz*-plane for the Vivaldi antenna (a), (c) without and with (b), (d) the PGMS.

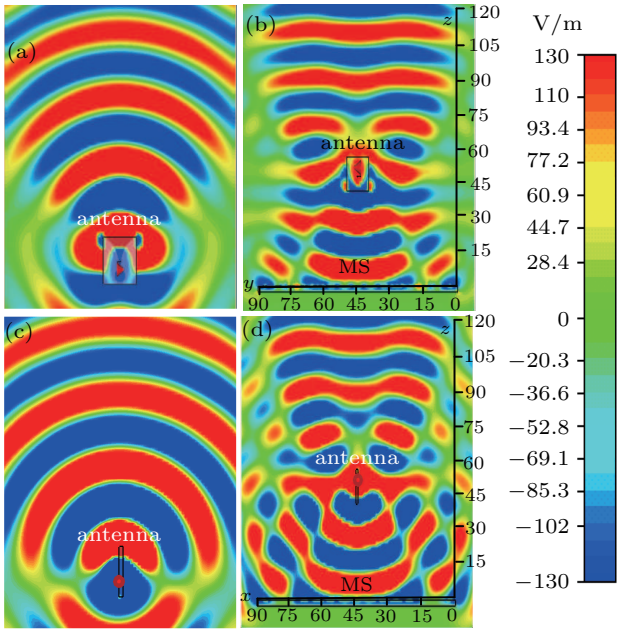


Fig. 8. (color online) Simulated electric field distribution at 18 GHz in (a), (b) *yoz*-plane and (c), (d) *xoz*-plane for the Vivaldi antenna (a), (c) without and with (b), (d) the PGMS.

Meanwhile, to clearly show the farfield performance enhancement by the reflected PGMS, the 3D radiation patterns at 15 GHz, 18 GHz, and 22 GHz are shown in Fig. 10. It can be concluded from the figure that the gain of the feed source is remarkably enhanced in a broad bandwidth and a pencil-shaped radiation pattern is achieved. Therefore, the PGMS can be applied for the planar antenna to improve gain and directivity.

In order to verify the simulation, a sample with an overall size of 90 mm×90 mm and 15×15 elements is fabricated as shown in Fig. 11(a). Besides, the designed Vivaldi antenna is fabricated and properly pasted on the center of the foam with the metasurface on the opposite so that the distance between the antenna and the PGMS is a constant of 33 mm.

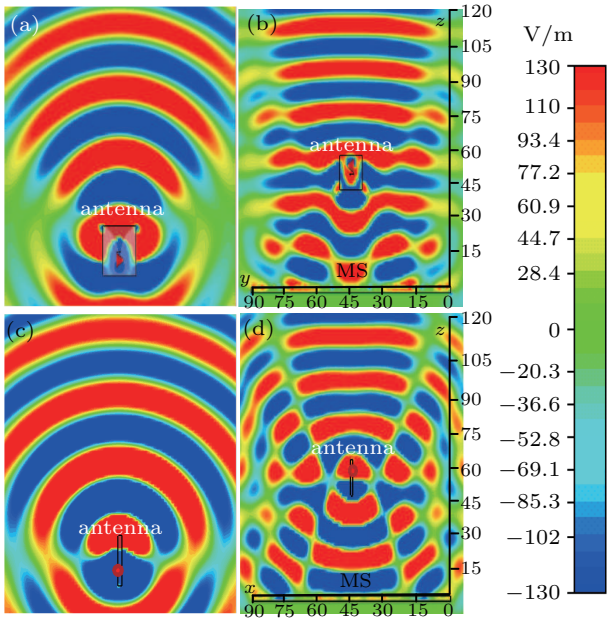


Fig. 9. (color online) Simulated electric field distribution at 22 GHz in (a), (b) *yoz*-plane and (c), (d) *xoz*-plane for the Vivaldi antenna (a), (c) without and with (b), (d) the PGMS.

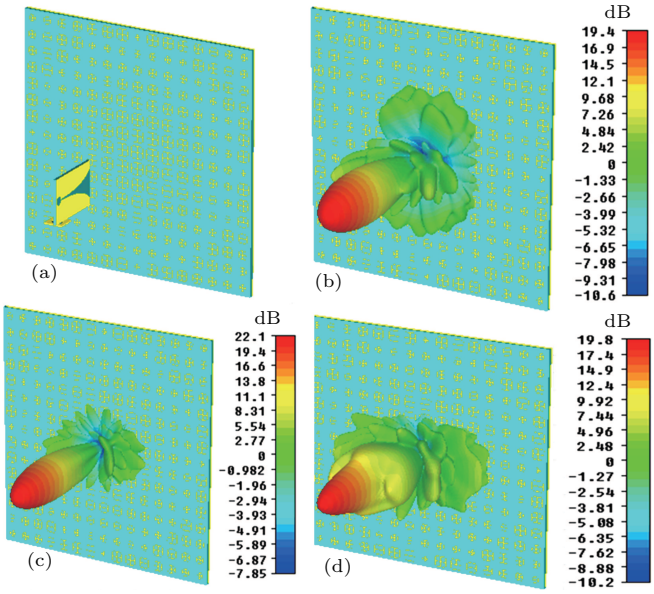


Fig. 10. (color online) (a) Simulated model for planar antenna; and 3D radiation patterns at (b) 15 GHz, (c) 18 GHz, (d) 22 GHz.

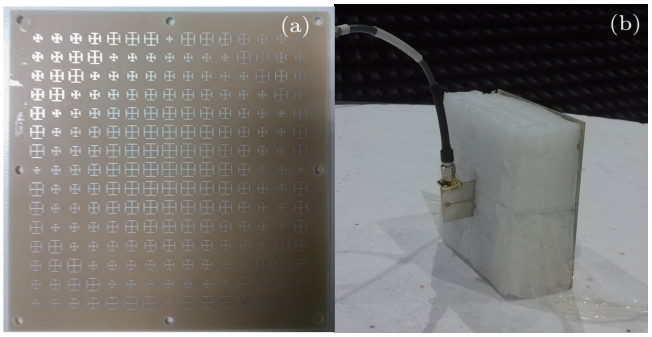


Fig. 11. Photographs of (a) metasurfaces and (b) planar high-gain antenna.

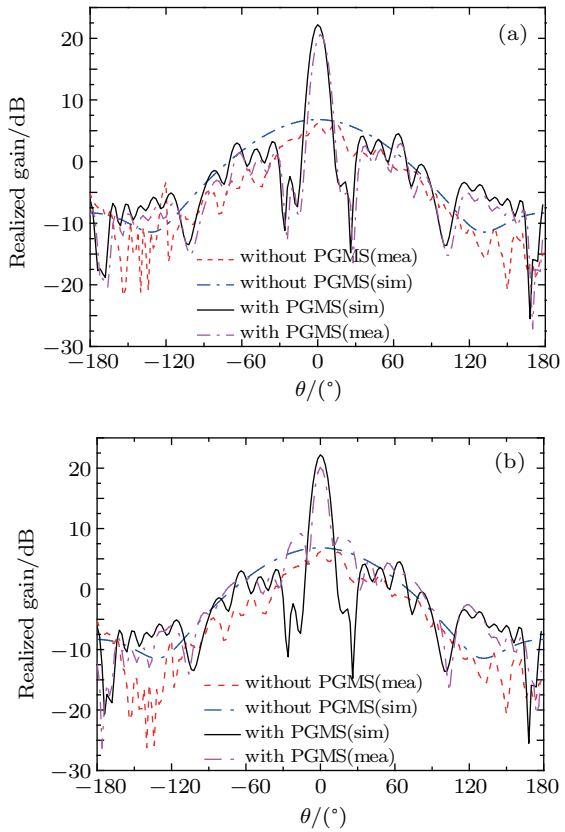


Fig. 12. (color online) Simulated and measured farfield radiation patterns at 18 GHz: (a) *xoz*-plane, (b) *yoz*-plane.

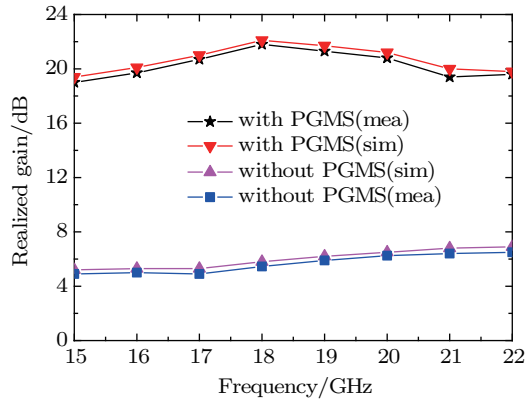


Fig. 13. (color online) Simulated and measured realized gain with/without PGMS from 15 GHz to 22 GHz.

For further verification, the simulated and measured radiation patterns in the *xoz*-plane and *yoz*-plane at 18 GHz are illustrated in Fig. 12. It is obvious that the proposed PGMS has considerably enhanced the gain of the Vivaldi antenna, with a peak gain enhancement of 15 dB relative to the bare Vivaldi antenna. Moreover, the 3-dB gain bandwidth is from 15 GHz to 22 GHz in Fig. 13. These measured results conform to the simulation, and the differences to the simulation results are mainly caused by the fabrication and measurement error. The high reflected efficiency and good focusing effect of the PGMS give rise to the favorable performances of the planar antenna.

4. Conclusion

We have proposed a broadband single layered reflected focusing phase-gradient metasurface and applied it in a high-gain planar antenna. The metasurface exhibits good focusing behavior from 15 GHz to 22 GHz, resulting in enhancing the directivity and gain of the antenna. Both simulation and test results show that the peak gain of the planar antenna is averagely enhanced by 16 dB in the 3-dB gain bandwidth of 15–22 GHz. Due to the thin thickness, polarization insensitivity, and broad bandwidth, the proposed metasurface opens up a new route for the applications of PGMS in the microwave band.

Acknowledgment

The authors would like to express their gratitude to China's North Electronic Engineering Research Institute for the fabrication.

References

[1] Shi Y, Yang K D, Yang Y X and Ma Y L 2015 *Chin. Phys. B* **24** 44102
[2] Liu G C, Li C and Fang G Y 2015 *Chin. Phys. B* **24** 14101
[3] Liu C and Wang Y H 2015 *Chin. Phys. B* **24** 10602
[4] Farmahini-Farahani M, Cheng J R and Mosallaei H 2013 *J. Opt. Soc. Am.* **30** 2365
[5] Yu N and Capasso F 2014 *Nat. Mater.* **13** 139
[6] Kildishev A V, Boltasseva A and Shalaev V M 2013 *Science* **339** 1232009
[7] Yu N, Genevet P, Kats A M, Aieta F, Tetienne J P, Capasso F and Gaburro Z 2011 *Science* **334** 333
[8] Pu M B, Chen P, Wang C T, Wang Y Q, Zhao Z Y, Hu C G, Huang C and Luo X G 2013 *AIP Advances* **3** 052136
[9] Wei Z Y, Cao Y, Su X P, Gong Z J, Long Y and Li H Q 2013 *Opt. Express* **21** 010739
[10] Ni X, Ishii S, Kildishev A V and Shalaev V M 2013 *Light Sci. Appl.* **2** 72
[11] Yu N, Genevet P, Kats A M, Aieta F, Tetienne J P, Capasso F and Gaburro Z 2011 *Science* **334** 333
[12] Aieta F, Genevent P, Kats M A, Yu N F, Blanchard R, Gaburro Z and Capasso F 2012 *Nano Lett.* **12** 4932
[13] Pors A, Nielsen M G, Eriksen R L and Bozhevolnyi S I 2013 *Nano Lett.* **13** 829
[14] Encinar J A 2001 *IEEE Trans. Antennas Propag.* **49** 1403
[15] Carrasco E, Encinar J A and Barba M 2008 *IEEE Trans. Antennas Propag.* **56** 2496
[16] Pozar D M 2007 *Electron. Lett.* **43** 148
[17] Yu A, Yang F, Elsherbeni A Z, Huang J and Kim Y 2012 *IEEE Trans.Antennas Propag.* **60** 1619